An atomic force microscope tip designed to measure time-varying nanomechanical forces

OZGUR SAHIN[1]*, SERGEI MAGONOV[2†], CHANMIN SU[2], CALVIN F. QUATE[3] AND OLAV SOLGAARD[3]

[1]Rowland Institute at Harvard, Cambridge, Massachusetts 02142, USA
[2]Veeco Instruments, Santa Barbara, California 93117, USA
[3]E. L. Ginzton Laboratory, Stanford University, Stanford, California 94305, USA
[†]Present address: Agilent Technologies, 4330 W. Chandler Boulevard, Chandler, Arizona 85226, USA
*e-mail: sahin@rowland.harvard.edu

Published online: 29 July 2007; doi:10.1038/nnano.2007.226

Tapping-mode atomic force microscopy (AFM), in which the vibrating tip periodically approaches, interacts and retracts from the sample surface, is the most common AFM imaging method. The tip experiences attractive and repulsive forces that depend on the chemical and mechanical properties of the sample, yet conventional AFM tips are limited in their ability to resolve these time-varying forces. We have created a specially designed cantilever tip that allows these interaction forces to be measured with good (sub-microsecond) temporal resolution and material properties to be determined and mapped in detail with nanoscale spatial resolution. Mechanical measurements based on these force waveforms are provided at a rate of 4 kHz. The forces and contact areas encountered in these measurements are orders of magnitude smaller than conventional indentation and AFM-based indentation techniques that typically provide data rates around 1 Hz. We use this tool to quantify and map nanomechanical changes in a binary polymer blend in the vicinity of its glass transition.

Phase changes and chemical compositional variations in materials on the nanoscale have been studied using various scanning force microscopy techniques. In these techniques, a force-sensing cantilever with a sharp tip is placed in continuous contact with the sample surface. Dynamical properties of the cantilever are adjusted depending on the material in contact with the tip. Examples of these techniques include ultrasonic force microscopy[1], force modulation microscopy[2], shear modulation force microscopy and lateral force microscopy[3,4]. These techniques typically provide a one-dimensional signal, such as a change in vibration amplitude or deflection, although the tip–sample interaction is affected by multiple parameters. As a result, extensive modelling and many assumptions are required to interpret the measurements. A drawback of these techniques occurs when operating the contact mode under large loading forces, where tip and sample damage are more likely to occur. This restricts the range of materials that can be studied and limits the spatial resolution of the measurements. Force curve methods in contact-mode and nanoindentation techniques based on atomic force microscopy (AFM) provide more reliable stiffness measurements[5,6], but low operation speeds (~1 s per measurement) and large loading forces limit their use.

Tapping-mode AFM has become the most widely used imaging method because the tip's interaction with the sample surface is relatively gentle, substantially eliminating plastic deformation and reducing the sample volume involved in the tip–sample interaction[7,8]. However, it has been difficult to extract material properties in the tapping mode. In this article, we present a specially designed AFM cantilever tip, the torsional harmonic cantilever (THC), which overcomes this difficulty.

In tapping-mode AFM, the cantilever is excited to vibrate at its resonant frequency and is brought close to the sample. Intermittent contact with the surface alters the amplitude and phase of the cantilever vibration. The vibrations are detected with an optical system where a laser beam reflects from the back of the cantilever and then falls onto a position-sensitive photodetector (Fig. 1). The laser spot moves up and down on the photodetector as the cantilever vibrates. A feedback mechanism adjusts the height of the cantilever base so that the vibration amplitude is maintained at a set-point value slightly below the free amplitude. As the cantilever is scanned across the surface, the feedback signal is used to map the topography of the sample surface.

The tapping cantilever vibrates approximately in a sinusoidal trajectory. The amplitude and phase of this trajectory are the two primary observables. Unfortunately, these quantities only provide time-averaged values of the tip–sample interaction forces[9,10]. Therefore, the information about how the interaction force varies as the tip undergoes its trajectory is lost to a large extent. The use of higher harmonic vibrations excited by the tip–sample forces would provide useful information[11–16]. There are, however, two major difficulties in this approach. First, the signal-to-noise ratios of the higher harmonic vibrations are not sufficient for practical measurements[17]. Second, the overall frequency response of the cantilever, required for translating harmonic vibration signals into harmonic forces acting on the tip, depends on the shape of the cantilever mode and the

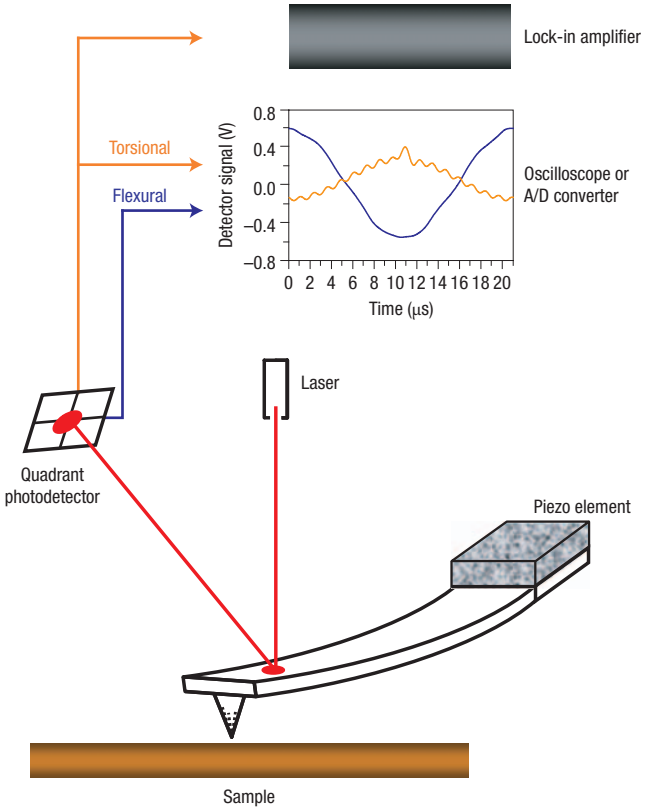

Figure 1 Schematic of the tapping-mode atomic force microscope and the experimental set up. The cantilever is vibrated with a piezo element at the resonance frequency. The up–down (flexural) and twisting (torsional) vibrations of the cantilever are detected by a quadrant photodetector that is sensitive to the position of the laser spot reflecting from the back side of the cantilever. The blue curve in the oscilloscope indicates the flexural oscillation and the orange curve indicates the torsional oscillation.

position of the laser spot[18]. It is very difficult to determine all of these parameters accurately. The THC enhances the signals at higher harmonics and provides a frequency response that can be accurately determined.

THE TORSIONAL HARMONIC CANTILEVER

The THC has a tip that is offset from the long axis of the cantilever (Fig. 2a). When it is vibrated in the tapping mode, tip–sample interaction forces generate a torque around the long axis of the cantilever and excite the torsional modes (Fig. 2b,d). Torsional deflections move the laser spot horizontally on the photodetector (Fig. 2c). As in the case of the conventional tapping-mode AFM, flexural (vertical) vibration signals are used for amplitude feedback to follow topography. Simultaneously, torsional vibration signals are used for the calculation of the time-resolved tip–sample interaction forces. The advantage of the use of torsional vibrations is explained in the next section, where we analyse the dynamics of the THC in the tapping mode.

DYNAMICS OF THE TORSIONAL HARMONIC CANTILEVER

Analysis of high-frequency torsional and flexural vibrations of the tapping cantilever requires modelling the cantilever as a continuum mechanical element with multiple vibration modes. We will follow the framework used by M. Stark and colleagues, which treats the tip–sample interaction as a feedback force on cantilever displacement[19]. This allows the tapping cantilever to be represented by a linear system (equivalent to the response of a cantilever fixed at the base and free near the tip). This cantilever is driven by two external forces: tip–sample forces and the driving force.

In the following analysis, the cantilever is represented as a linear time-invariant system with a transfer function $\mathbf{G}$ that relates the cantilever displacement $\Psi(x, y, t)$ to the total force acting on it, $f(x, y, t) = f_{\text{drive}} + f_{\text{tip}}$, hence $\Psi(x, y, t) = \mathbf{G}f(x, y, t)$. The optical detection system (quadrant photodetector) is represented with the operator $\mathbf{C}$, which relates the vertical and horizontal detector signals $\mathbf{s}_x$ and $\mathbf{s}_y$ to the cantilever displacement by $\mathbf{s}_x = \mathbf{C}_x\Psi$ and $\mathbf{s}_y = \mathbf{C}_y\Psi$. We note that the photodetector signal is directly proportional to the slope of the cantilever, therefore $\mathbf{C}_x = \partial/\partial x$ and $\mathbf{C}_y = \partial/\partial y$, evaluated at the location of the laser spot. With these definitions, the relationship between the detector signals and the forces on the cantilever can be written as

$$\mathbf{s} = \mathbf{CG}(f_{\text{drive}} + f_{\text{tip}}) \tag{1}$$

where $\mathbf{s}$ is a vector with two components representing the vertical and horizontal signals of the detector. In principle, matrices $\mathbf{G}$ and $\mathbf{C}$ can be separated into flexural and torsional components. This is equivalent to saying that the flexural modes only result in vertical signals in the detector, and the torsional modes only horizontal signals. (Note that the actual experimental conditions slightly deviate from these two conditions due to the crosstalk from large vertical deflections coupling into lateral signals.) Furthermore, the driving force will only excite the flexural modes. We assume we can neglect the effect of in-plane forces between the tip and the sample for the torsional vibrations. In the experiments we scan the cantilever along the longitudinal axis so that in-plane forces do not generate torque around that axis. Also, the lateral tip motion due to torsional oscillations is estimated to be below 1 Å, considerably smaller than the typical sample indentation depths. Based on these assumptions we can write

$$\mathbf{s}_X = \mathbf{C}_X\mathbf{G}_X(f_{\text{drive}} + f_{\text{tip}}) = \mathbf{H}_X(f_{\text{drive}} + f_{\text{tip}}) \tag{2}$$

and

$$\mathbf{s}_Y = \mathbf{C}_Y\mathbf{G}_Y f_{\text{tip}} = \mathbf{H}_y f_{\text{tip}} \tag{3}$$

The operators $\mathbf{G}_X$ and $\mathbf{G}_Y$ represent the combined response of flexural and torsional modes, respectively. Note that equation (3) only deals with f_{tip}, because the torsional vibrations are only excited by the tip–sample forces. This equation can be used to obtain f_{tip} from $\mathbf{s}_Y$ by estimating the transfer function corresponding to $\mathbf{H}_Y$ and its inverse. The response of torsional modes $\mathbf{G}_Y$ can be estimated with a simple damped harmonic oscillator that has a resonance frequency of the first torsional mode and the corresponding quality factor. The operator $\mathbf{C}_Y$ is estimated with a scalar multiplier c_{optical} that corresponds to the bending angle of the cantilever for a unit tip displacement in the torsional mode. The resulting transfer function $H_Y(\omega)$ is given by

$$H_y(\omega) = c_{\text{optical}} \frac{\omega_T^2/K_T}{\omega_T^2 - \omega^2 + i\omega\omega_T/Q_T}, \tag{4}$$

where ω is the angular frequency, ω_T is the torsional resonance frequency, and Q_T and K_T are the quality factor and effective

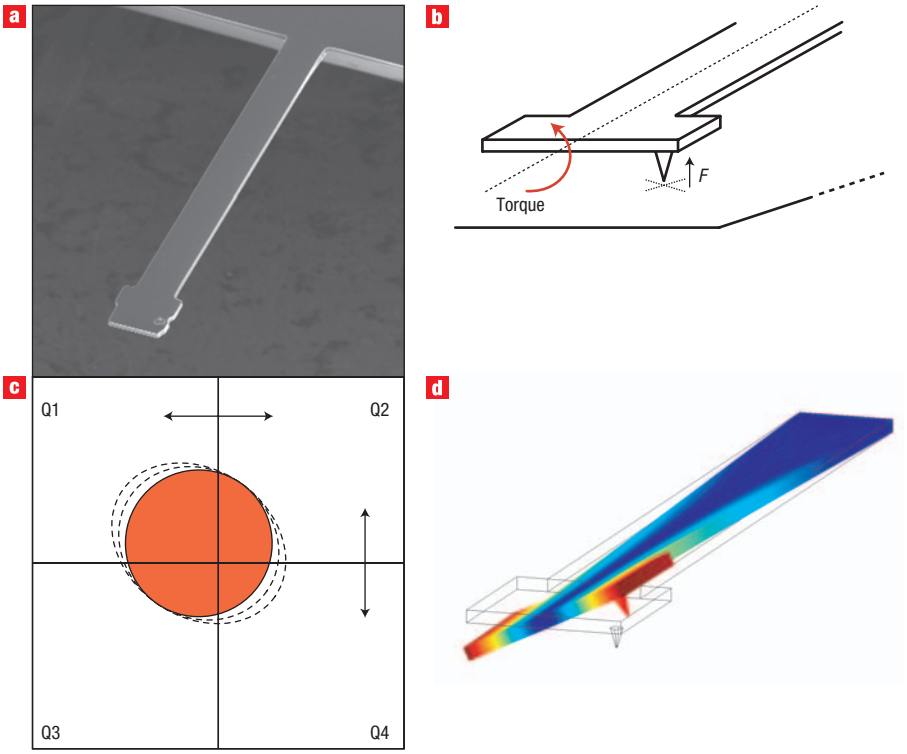

Figure 2 Design of the torsional harmonic cantilever with an off-axis tip. a, A scanning electron micrograph image of a torsional harmonic cantilever. The cantilever is 300 μm long, 3 μm thick and nominally 30 μm wide (50 μm near the free end). The tip is offset 15 μm from the centre of the cantilever. **b**, An illustration of the THC interacting with the surface. The offset position of the tip results in a torque around the axis of the cantilever. **c**, An illustration of the laser spot on the four-quadrant position-sensitive photodetector. The optical power difference (Q1 + Q2) − (Q3 + Q4) is proportional to vertical cantilever deflection, and (Q1 + Q3) − (Q2 + Q4) is proportional to torsional angle. **d**, Simulated first torsional mode shape of a THC fixed at the base. This mode is excited when the tip hits the surface.

spring constant of the torsional resonance. Once this transfer function is calibrated and $\mathbf{s_Y}$ is sampled with a data acquisition card, equation (3) can be numerically solved to obtain f_{tip}. Details of the numerical calculations and the calibration of the parameters that determine H_Y are described in the Methods section.

The two important parameters describing the transfer function H_Y are the gain and the bandwidth. The gain is determined by $c_{optical}/K_T$ and the bandwidth is limited by ω_T. Larger gain enhances sensitivity, and larger bandwidth provides better time resolution.

Calculated transfer functions corresponding to $H_X(\omega)$ and $H_Y(\omega)$ and experimentally measured vibration spectra of a THC tapping on a polystyrene sample are plotted in Fig. 3 to demonstrate the advantages of the torsional vibrations. The flexural frequency response shows multiple resonances corresponding to the fundamental and higher-order modes at frequencies up to 20 Hz. (The dips and zeros in the frequency response arise due to cancellation of the neighbouring modes.) In the same frequency range, there is only one torsional resonance frequency. These curves show that the torsional vibrations provide a larger response (sensitivity) over a wide range of frequencies (bandwidth). The improved sensitivity is due to the larger $c_{optical}$. In particular, because the moment arm in the torsional direction is much shorter than the length of the cantilever, these vibrations result in larger angular deflections and have a lower effective spring constant K_T than the higher-order flexural modes.

The vibration spectra measured while tapping on a polystyrene sample (Fig. 3b,c) show that there is a dominant peak at the drive frequency (51.2 kHz) in the flexural spectrum. The other peaks are the higher harmonics that are excited by the periodic tip–sample forces, but beyond 300 kHz these harmonics have low signal-to-noise ratios. This illustrates the drawback of the use of flexural harmonics for the recovery of time-resolved tip–sample forces. In contrast, the torsional vibration spectrum shows peaks with good signal levels at the higher harmonics up to 1 MHz. Note that there is also a good degree of agreement between the calculated frequency response and the measured torsional spectrum. These results show that the torsional vibrations of a THC recover the high-frequency force components necessary to reconstruct time-resolved tip–sample forces.

RECONSTRUCTING THE TIP–SAMPLE FORCE WAVEFORM

We recorded the flexural and torsional vibration signals with a data acquisition card. The vibration signals are quasi-periodic in the tapping mode. Therefore we averaged the data over 12 oscillation cycles to further reduce the noise. This results in a measurement bandwidth of ∼4 kHz. Figure 4a shows a plot of the data obtained on a highly oriented pyrolytic graphite sample. The flexural signal is approximately a sinusoid at the drive frequency, with weak higher harmonic vibrations. The torsional vibrations exhibit a more complicated waveform. When the tip hits the sample (the lowest point in the flexural waveform), the cantilever bends torsionally in proportion to the torque generated by the tip–sample forces (orange arrow). After this impact, the

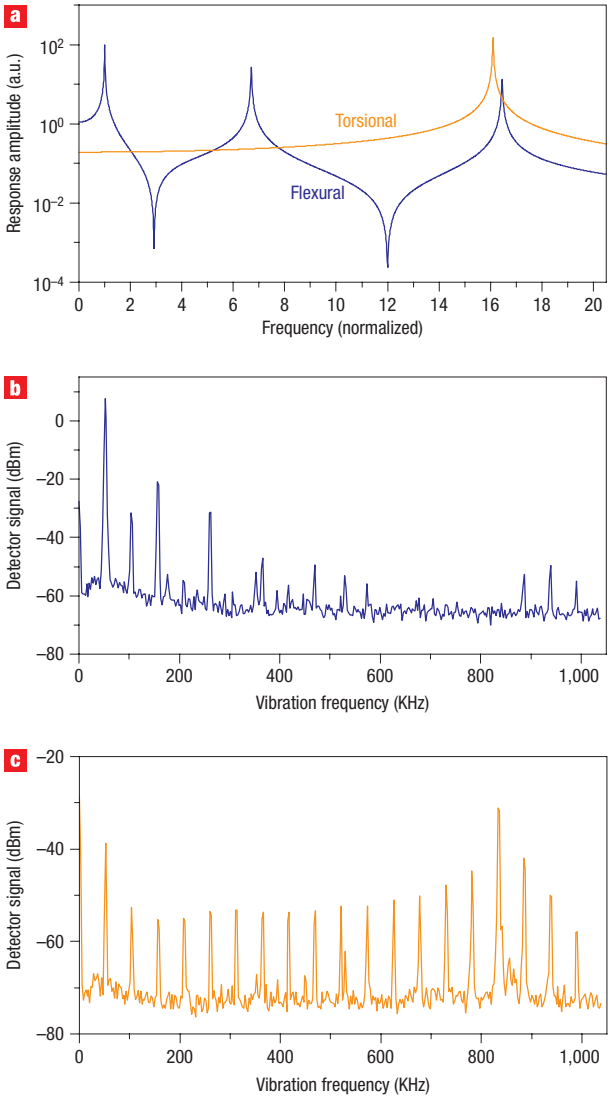

Figure 3 Frequency response and vibration spectra of a torsional harmonic cantilever. a, The frequency response of flexural (blue) and torsional (orange) modes of a THC. The frequency axis is normalized so that the first flexural resonance frequency is one. **b**,**c**, Flexural (**b**) and torsional (**c**) vibration spectra of a THC tapping on a polystyrene sample. The first peak of the flexural spectrum in **b** is at the driving frequency and is the largest component of the cantilever motion. All other flexural and torsional peaks are the higher harmonics generated by the tip–sample interaction force. The torsional peaks show much better signal levels at higher frequencies. Note the similarity between the magnitudes of the peaks in the torsional spectrum and the corresponding frequency response curve in **a**.

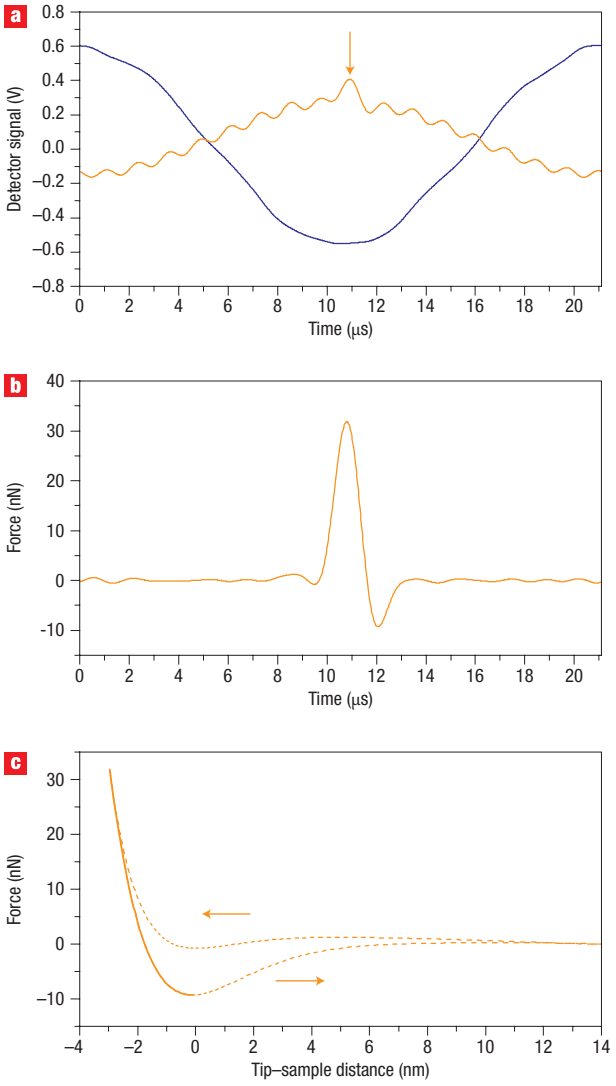

Figure 4 Reconstructing the tip–sample force waveform. a, Oscilloscope traces of the periodic flexural (blue) and torsional (orange) vibration signals at the position-sensitive detector, obtained on graphite. **b**, Time-resolved tip–sample force measurements calculated on graphite. **c**, The same data as in **b**, plotted against tip–sample distance. Negative distances mean that the sample is indented. Arrows indicate the direction of motion. The solid part of the curve marks the points between the largest sample indentation and breaking of the contact on the retraction portion of the curve.

cantilever exhibits slowly decaying torsional oscillations with a frequency close to the torsional resonance frequency. This behaviour is also reflected in the torsional vibration spectrum given in Fig. 3c as a pronounced increase in the magnitudes of the peaks around the 15th to 17th harmonics.

Figure 4b plots the time-resolved tapping-force waveform obtained on graphite calculated according to equation (3) using the torsional deflection signal in Fig. 4a. The waveform is in the shape of a pulse where the positive forces are the repulsive tip–sample interactions that arise as the tip indents the sample. The vertical position of the tip is approximately a sinusoid with a known amplitude and phase. We can therefore eliminate the time variable and plot all the force measurements in Fig. 4b against tip–sample distance, as shown in Fig. 4c. Hereafter, these curves will be referred to as time-resolved tapping-force curves. There are two force values recorded for a given tip–sample distance: one for the approaching tip and one for the retracting tip. These time-resolved tapping force curves reveal the richness of the tip–sample interaction in the tapping mode. The rate of increase in the repulsive forces during the indentation is proportional to the stiffness of the sample. The magnitudes of the negative forces depend on the van der Waals parameters of the tip–sample ensemble, as well as the capillary forces due to a liquid meniscus acting on the tip[20]. The measurements also reveal a hysteresis in the attractive forces on approach and retraction of the tip, with a

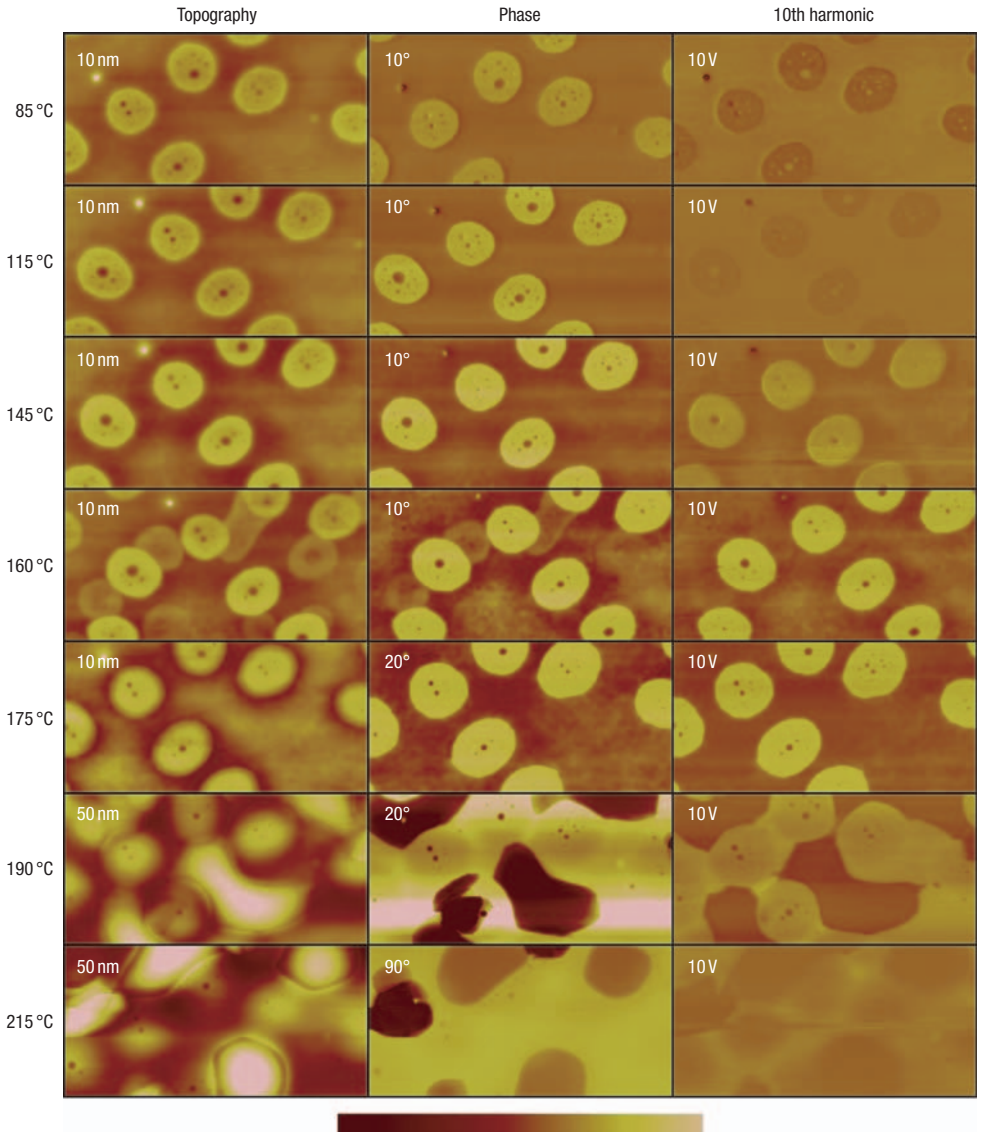

Figure 5 Changes in the mechanical properties of a polymer blend near the glass transition. Topography, phase and tenth-harmonic images of a thin polymer film composed of PS and PMMA recorded at different temperatures. The circular features are PMMA, and the matrix is PS. Brighter colour (more yellow) represents larger height, phase or harmonic amplitude. The scan area is 2.5 × 5 μm. The colour bar represents different height and phase ranges at each temperature (the range is given in the top left corner of each panel). For the harmonic images, the colour bar represents a 10 V lock-in output signal at all temperatures. Note that height and phase contrast increases with temperature, whereas the harmonic contrast is first increasing and then decreasing.

much larger attractive force associated with the unloading portion of the indentation forces (solid line in Fig. 4c).

The variation in the repulsive force with sample indentation depends on the material properties of the tip and the sample, as well as the shape of the tip. In stiffer materials, a larger loading force is required to produce a given depth of indentation. An approximate model for macroscopic bodies describing the indentation of a flat surface with a spherical probe predicts that the forces vary with the following relationship[21]:

$$F_{\mathrm{tip}} = \frac{4}{3} E^{*} \sqrt{R}\, d^{3/2} + F_{\mathrm{adh}}, \qquad (5)$$

where F_{tip} is the tip–sample force, E^{*} is the reduced Young's modulus, R is the tip radius, d is the indentation depth and F_{adh} is the tip–sample adhesion force. This formula is valid for contacts where adhesion is either constant during the indentation (Derjaguin-Muller-Toporov model) or negligible (Hertz model)[21]. In general, adhesion plays an important role in contact mechanics and the formula relating forces to indentations takes on a more complicated form. We worked with a THC that has a relatively sharp tip to decrease the role of adhesive forces. (Note, the second THC was fabricated with a process similar to that used for commercial AFM cantilevers that results in a 7-nm tip radius, characterized by blind reconstruction from the AFM image of a sample with sharp edges.) For a given tip, the differences between materials arise only in the reduced Young's modulus and the adhesion force. Although the validity of macroscopic models for nanoscale contacts is yet to be determined[22], the results presented hereafter are in agreement

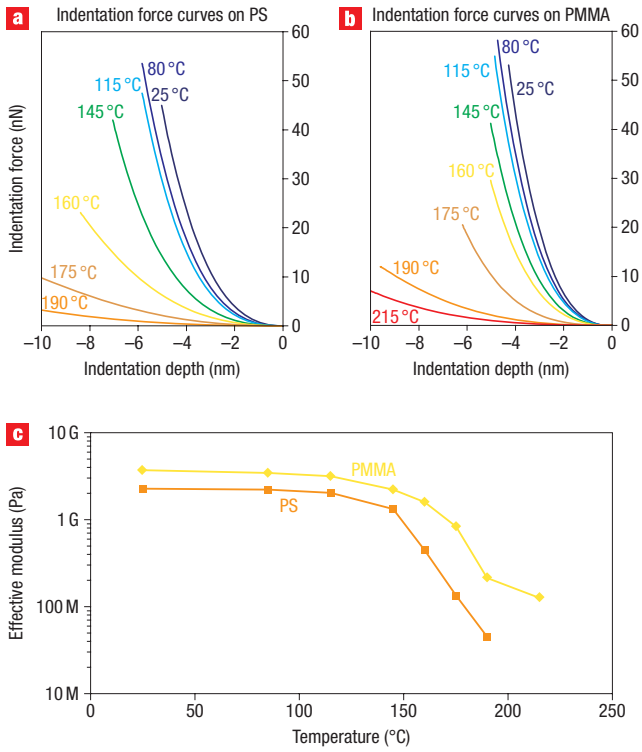

Figure 6 Indentation forces as a function of temperature in a polymer blend. a,**b**, Time-varying force measurements plotted against sample indentation for polystyrene (**a**) and PMMA (**b**). **c**, Corresponding effective Young's modulus values are calculated by fitting the force curves to equation (5).

with the above relationship, at least for indentations comparable to or less than the tip radius.

TORSIONAL HARMONIC IMAGES

The multidimensional signal in Fig. 3 contains information about many properties of the sample surface. A simple method to produce qualitative maps of stiffness is to record the amplitude of a single higher harmonic[13,23,24]. Theoretical studies of the higher harmonic response indicate that the amplitude of a higher harmonic depends on the stiffness of the sample; however, a proper choice of the higher harmonic is important[25]. The THC has good signal levels at torsional harmonics up to the torsional resonance frequency, so it provides the flexibility to image with any of these harmonics to produce the corresponding torsional harmonic image of the surface. We generate torsional harmonic images by using a lock-in amplifier that is tuned to the frequency of a particular higher harmonic.

With topography, phase and torsional harmonic images, we have investigated the structural properties of an approximately 50-nm-thick binary polymer film on a silicon substrate near the glass transition temperature of the two components, polystyrene (PS) and polymethylmethacrylate (PMMA). The PS and PMMA have distinct glass transition temperatures (around 100 °C and 130 °C, respectively) and form sub-micrometre domains within the film. Each polymer component transitions from a stiff glassy phase to a rubbery phase at its respective glass transition temperature. In the temperature range between the glass transitions of PS and PMMA, the regions of rubbery PS phase will be more compliant than the glassy PMMA regions. Using torsional harmonic images, we can observe the glass transitions of individual components of the composite polymer film.

Figure 5 shows the topography, phase and tenth torsional harmonic images obtained at temperatures between 85 and 215 °C. Images at different temperatures correspond to approximately the same position on the sample, though some shift results from thermal drift in the system. Lateral resolution, however, is not affected by thermal drift because the imaging time is in the order of seconds, and the drift is $\sim$0.5 nm min^{-1}. The tenth harmonic was chosen because it is close to the torsional resonance frequency. At low temperatures, the two material components are distinguishable in all three images. PMMA forms the round features and PS forms the matrix.

The topography of the surface shows height variations between the two components at low temperatures. However, dramatic changes in height are observed at high temperatures. Above 190 °C, the boundaries between the different polymer components become unclear. At elevated temperatures, the rubbery material gains liquid-like mobility, and flows and rearranges so that it forms round (droplet-like) features on the surface. This leads to larger but smoother topographical variations.

Phase images also show dramatic changes with temperature. The phase of the cantilever oscillations depends on the energy dissipation during the tip–sample contact[9]. Formation and disruption of a liquid neck between the tip and the sample, hysteresis in adhesion forces, and viscosity of the sample are the major energy-dissipation mechanisms. In particular, on a compliant sample, attractive forces between the tip and the sample are strong enough to pull the sample locally and raise it above its equilibrium level. Once the contact is broken, the mechanical energy stored in the raised sample is dissipated. Because of this, the polymer components dissipate energy more at elevated temperatures where they are more compliant. As well as this mechanism, increased viscosity in the rubbery phase also leads to increased energy dissipation. The increase in the contrast in the phase images near the first transition at 160 °C is primarily due to these effects; however, the contrast becomes larger even when both materials are in the rubbery phase. This illustrates one of the limitations of phase imaging. In general, phase images identify different material components; however, interpreting the nature of the contrast is difficult owing to the multiple mechanisms involved[26].

Below 160 °C, the domains of PS and PMMA are distinguishable in the torsional harmonic images, but the contrast is small. This is because the two materials have similar mechanical properties in their glassy phases. At 160 °C and 175 °C, the contrast between the PS and PMMA domains increases in the torsional harmonic image. A reduction in the amplitude of the harmonic signal is recorded on the PS matrix. According to ref. 25, a reduction in higher harmonic amplitudes results from an increased mechanical compliance of a material. This indicates the glass transition of PS. The contrast is reduced at 190 °C and almost completely disappears at 215 °C, as the PMMA gradually transitions to the rubbery phase. At 215 °C, both materials are in the rubbery phase, the harmonic amplitude near the PMMA and PS is small, and there is little contrast between the two materials. The torsional harmonic images provide a qualitative picture of the mechanical changes in the sample that is not directly accessible from the phase or topography images; however, a better understanding of the changes in the samples can be obtained by analysing the time-varying tip–sample forces.

QUANTITATIVE NANOMECHANICAL MEASUREMENTS

The time-resolved tapping-force measurements are capable of providing a more detailed and potentially quantitative

understanding of the changes observed on the polymer film by generating indentation force versus indentation depth curves (solid part of the curve in Fig. 4c). In Fig. 6, we plot these curves recorded while the cantilever is scanning over the PS and PMMA regions at each temperature (see Supplementary Information, text and Fig. S3, for complete time-resolved tapping-force curves). The slopes of the indentation forces gradually decrease with increasing temperature. This indicates that both materials are becoming increasingly compliant at elevated temperatures. In order to quantify these changes we use equation (5) to calculate the corresponding E^* values based on curve fitting with the assumption of a spherical tip with 7-nm radius. These values are plotted against temperature in Fig. 6c. At room temperature, the Young's modulus of PS and PMMA is measured as 2.3 GPa and 3.7 GPa, respectively, both of which are in the range of typical bulk values for these materials. The two polymers exhibit only a small reduction in stiffness at temperatures up to 115 °C. However, at higher temperatures, stiffness of both materials decreases by almost two orders of magnitude owing to the glass transition. According to these results, the apparent glass transition temperatures of the PS and PMMA are approximately 160 °C and 180 °C, respectively. The glass transition of PS occurs at lower temperatures compared with PMMA, as expected. At temperatures beyond the glass transition, these materials are viscoelastic, and indentation forces contain rate-dependent components that are not accounted for in equation (2), resulting in deviations from the model.

The relatively high transition temperatures are expected consequences of the frequency dependence of the material response around the glass transition[27,28]. With an increase in the measurement frequency, the glass transition temperature shifts towards higher temperatures at a rate of 5–10 °C per frequency decade. We note that our technique measures the mechanical properties at the harmonic frequencies (50–1,000 kHz), whereas the glass transitions of bulk materials are typically determined through thermal measurements or dynamic mechanical measurements at frequencies below 100 Hz (ref. 27).

CONCLUSIONS

The THC allows detailed mechanical measurements in the tapping mode, thereby enabling the study of a wide range of materials. The torsional harmonic images allow qualitative mapping of mechanical property variations, and the time-resolved tapping-force curves provide a detailed and quantifiable understanding of the changes observed on the surface. The time-resolved tapping-force measurements are performed within 250 μs, with a few nanometres of sample indentation and peak loading forces around 10 nN. Our new method has the inherent nanometre-scale lateral resolution of the tapping-mode AFM. These results represent orders of magnitude improvements in temporal resolution, spatial resolution, indentation and mechanical loading compared to conventional tools. With high operating speed, increased force sensitivity and excellent lateral resolution, our tool facilitates practical mapping of nanomechanical properties.

MATERIALS AND METHODS

EXPERIMENTAL SETUP

We used a commercial AFM system (Multimode series, equipped with Nanoscope 4 controller, signal break-out box, and torsional vibration detection electronics). Also used were an additional lock-in amplifier (Stanford Research Systems, SRS-844), a digital oscilloscope and a data acquisition card (NI DAQ, S-series). The sample was placed on a commercially available controlled heating stage. The cantilever was maintained at the same temperature as the sample.

TAPPING-MODE OPERATION PARAMETERS

The set-point and free vibration amplitudes for the measurements in Fig. 3 were 40 nm and 60 nm (first THC, $K = 2.4$ N m^{-1}, $f_0 = 47.4$ kHz, $Q = 55$). The set-point and free vibration amplitudes for the measurements in Figs 4 and 5 were 70 nm and 100 nm (second THC, $K = 6$ N m^{-1}, $f_0 = 50.8$ kHz, $Q = 91$). The drive frequency (50.5 kHz) for the imaging was chosen to be slightly below resonance frequency. This favours repulsive-mode operation. Scan rate during the imaging was chosen to be 1 Hz. The bandwidth used for lock-in detection of torsional harmonics was 3 kHz.

CALIBRATION OF THE TRANSFER FUNCTION $H_Y(\omega)$

The torsional resonance frequency ω_T and the corresponding quality factor Q_T were determined by the frequency-tuning software that comes with the AFM system ($Q_T = 800$ and $\omega_T = 809.1$ kHz for the first THC, and $Q_T = 1{,}050$ and $\omega_T = 528.0$ kHz for the second THC). The effective torsional spring constants of the cantilevers near the offset tip were measured by a vibrometer ($K_T = 550$ N m^{-1} for the first THC and $K_T = 480$ N m^{-1}). The optical gain $c_{optical}$ for torsional deflections was determined in two steps. First, the optical gain for the fundamental vertical mode (detector voltage for a unit tip displacement in this mode) was measured by obtaining force–distance curves in the tapping mode. Second, we multiplied this value by a geometrical factor that corresponds to the ratio of the slopes on the cantilever for a unit tip displacement in the torsional mode and flexural mode. The geometrical factor is estimated from the mode shapes of a rectangular cantilever. We neglect the frequency dependence of the optical gain because the cutoff frequency of the photodetector is around 3 MHz.

SAMPLING AND PROCESSING OF DETECTOR SIGNALS

The flexural and torsional (vertical and lateral) signals generated by the quadrant photodetector were low-pass-filtered with a cutoff frequency of 2 MHz, and were continuously downloaded to a computer with the data acquisition card. A Labview program was used to perform digital signal processing in order to obtain time-resolved forces. In this program, data were divided into packets where each packet has a number of samples that correspond to 12 oscillation cycles (first THC) or 120 oscillation cycles (second THC). For each data packet, discrete Fourier transform was calculated, and equation (3) was solved for f_{tip} in the frequency domain with the following equation:

$$f_{tip}(j) = \frac{1}{N}\sum_{k=1}^{N} H_Y^{-1}(\omega_k) S_Y(\omega_k) e^{i\omega_k(j-1)} \qquad (6)$$

Here, $S_Y(\omega_k)$ is the discrete Fourier transform of the sampled torsional deflection signal, H_Y^{-1} is the inverse of the transfer function given in equation (4), N is the number of data points per period and $f_{tip}(j)$ is the discrete form of tip–sample forces. Note that H_Y^{-1} diverges at frequencies much larger than the torsional resonance frequency. We introduce a cutoff frequency in the calculations that is slightly above the torsional resonance frequency to solve this issue (we use up to 20 harmonics for the first THC and 13 harmonics for the second THC). In order to represent $f_{tip}(j)$ with a larger number of points (resampling), we extend $S_Y(\omega_k)$ by zero padding beyond the cutoff frequency of the calculations. In that case, equation (6) is used with the final N value. The force waveforms presented in this work are resampled at 512 points per period.

The biggest source of error in these calculations is the crosstalk between the detector signals. The vertical channel has a large signal component at the drive frequency, which appears at the lateral channel as a crosstalk. We use a curve-fitting procedure to estimate and subtract the crosstalk signal from the waveform calculated by equation (6) (see Supplementary Information). The deviation in the final effective modulus estimates is approximately 5% for the nominal values around 1 GPa, and it gradually increases to 20% on samples around 50 MPa.

SAMPLE PREPARATION

Graphite Freshly cleaved highly oriented pyrolytic graphite was used.

Blended polymer film We used polystyrene ($M_w = 81$ K) and polymethylmethacrylate ($M_w = 73$ K and 81 K). Both are products of Polymer Source. The polymers were dissolved in hot toluene and cast as a thin film on Si substrate. The thickness of the film was 40–50 nm as estimated by AFM height measurements of a scratch made on this film by a sharp copper needle.

Received 20 October 2006; accepted 28 June 2007; published 29 July 2007.

References

1. Yamanaka, K., Ogiso, H. & Kolosov, O. Ultrasonic force microscopy for nanometer resolution subsurface imaging. *Appl. Phys. Lett.* **64,** 178–180 (1994).
2. Maivald, P. *et al.* Using force modulation to image surface elasticities with the atomic force microscope. *Nanotechnology* **2,** 103 (1991).
3. Ge, S. *et al.* Shear modulation force microscopy study of near surface glass transition temperatures. *Phys. Rev. Lett.* **85,** 2340–2343 (2000).
4. Dinelli, F., Buenviaje, C. & Overney, R. M. Glass transition measurements on heterogeneous surfaces. *Thin Solid Films* **396,** 138–144 (2001).
5. Oliver, W. C. & Pharr, G. M. An improved technique for determining hardness and elastic-modulus using load and displacement sensing indentation experiments. *J. Mater. Res.* **7,** 1564–1583 (1992).
6. Vanlandingham, M. R. *et al.* Nanoscale indentation of polymer systems using the atomic force microscope. *J. Adhesion* **64,** 31–59 (1997).
7. Zhong, Q., Inniss, D., Kjoller, K. & Elings, V. B. Fractured polymer/silica fiber surface studied by tapping mode atomic force microscopy. *Surf. Sci.* **280,** L688–L692 (1993).
8. Klinov, D. & Magonov, S. True molecular resolution in tapping-mode atomic force microscopy with high-resolution probes. *Appl. Phys. Lett.* **84,** 2697–2699 (2004).
9. Cleveland, J. P., Anczykowski, B., Schmid, A. E. & Elings V. B. Energy dissipation in tapping-mode atomic force microscopy. *Appl. Phys. Lett.* **72,** 2613–2615 (1998).
10. Paulo, A. S. & Garcia, R. Unifying theory of tapping-mode atomic force microscope *Phys. Rev B.* **66,** 041406 (2002).
11. Hillenbrand, R., Stark, M. & Guckenberger, R. Higher-harmonics generation in tapping-mode atomic-force microscopy: Insights into the tip–sample interaction. *Appl. Phys. Lett.* **76,** 3478–3480 (2000).
12. Stark, R. W. & Heckl, W. M. Fourier transformed atomic force microscopy: tapping mode atomic force microscopy beyond the Hookian approximation. *Surf. Sci.* **457,** 219–228 (2000).
13. Crittenden, S., Raman, A. & Reifenberger, R. Probing attractive forces at the nanoscale using higher-harmonic dynamic force microscopy. *Phys. Rev. B* **72,** 235422 (2005).
14. Legleiter, J., Park, M., Cusick, B. & Kowalewski, T. Scanning probe acceleration microscopy (SPAM) in fluids: mapping mechanical properties of surfaces at the nanoscale. *Proc. Natl Acad. Sci. USA* **103,** 4813–4818 (2006).
15. Hembacher, S., Giessibl, F. J. & Mannhart, J. Force microscopy with light-atom probes. *Science* **305,** 380–383 (2004).
16. Stark, M., Stark, R. W., Heckl, W. M. & Guckenberger, R. Inverting dynamic force microscopy: from signals to time-resolved interaction forces. *Proc. Natl Acad. Sci. USA* **99,** 8473–8478 (2002).
17. Rodriguez, T. R. & Garcia, R. Tip motion in amplitude modulation (tapping-mode) atomic-force microscopy: comparison between continuous and point-mass models. *Appl. Phys. Lett.* **80,** 1646–1648 (2002).
18. Stark, R. W. Optical lever detection in higher eigenmode dynamic atomic force microscopy. *Rev. Sci. Instrum.* **75,** 5053–5055 (2004).
19. Stark, R. W., Schitter, G., Stark, M., Guckenberger, R. & Stemmer, A. State-space model of freely vibrating and surface-coupled cantilever dynamics in atomic force microscopy. *Phys. Rev. B* **69,** 085412 (2004).
20. Zitzler, L., Herminghaus, S. & Mugele, F. Capillary forces in tapping-mode atomic force microscopy *Phys. Rev. B* **66,** 155436 (2002).
21. Isrelachvili, J. *Intermolecular and Surface Forces* (Academic Press, London, 2003).
22. Luan, B. Q. & Robbins, M. O. The breakdown of continuum models for mechanical contacts. *Nature* **435,** 929–932 (2005).
23. Stark, R. W. & Heckl, W. M. Higher harmonics imaging in tapping-mode atomic-force microscopy. *Rev. Sci. Instrum.* **74,** 5111–5114 (2003).
24. Sahin, O. *et al.* High-resolution imaging of elastic properties using harmonic cantilevers. *Sensor. Actuat. A* **114,** 183–190 (2004).
25. Sahin, O., Atalar, A., Quate, C. F. & Solgaard, O. Resonant harmonic response in tapping-mode atomic force microscopy. *Phys. Rev. B.* **69,** 165416 (2004).
26. Garcia, R. *et al.* Identification of nanoscale dissipation processes by dynamic atomic force microscopy. *Phys. Rev. Lett.* **97,** 016103 (2006).
27. Ward, I. M. & Sweeney, J. *An Introduction to the Mechanical Properties of Solid Polymers* (Wiley, Chichester, 2004).
28. Dinelli, F., Buenviaje, C. & Overney, R. M. Glass transitions of thin polymeric films: speed and load dependence in lateral force microscopy. *J. Chem. Phys.* **113,** 2043–2048 (2000).

Acknowledgements

We thank N. Yerina of Veeco Instruments for preparing the polymer samples. The authors acknowledge support from the Center for Probing the Nanoscale (CPN), and NSF NSEC, NSF Grant No. PHY-0425897. O. Sahin acknowledges support from the Rowland Junior Fellows Program.
Correspondence and requests for materials should be addressed to O. Sahin.
Supplementary information accompanies this paper on www.nature.com/naturenanotechnology.

Competing financial interests

The authors declare competing financial interests: details accompany the full-text HTML version of the paper at www.nature.com/naturenanotechnology.